Supersonic Flow in the Blade Channel of the Nozzle with a Rotary Diaphragm at Small Degrees of Opening

Oleksandr Zhyrkov[1], Oleksandr Usatyi[2], Olena Avdieieva[2(✉)], and Yuri Torba[1]

[1] SE Ivchenko-Progress, 2 Ivanova Street, Zaporozhye 69068, Ukraine
[2] National Technical University "Kharkiv Polytechnic Institute", 2 Kyrpychova Street, Kharkiv 61002, Ukraine
o.avdieieva@gmail.com

Abstract. The article presents a study of the flow of supersonic flow in the interscapular duct of a nozzle with a rotating aperture at low degrees of opening. Modeling and calculation of the working fluid flow were carried out using the Fluent software package. The construction of computational domains, limited by one interscapular channel, for different degrees of opening of the nozzle diaphragm has been carried out. Grids for computational domains have been built. A numerical study of the flow in the interscapular channel of the C-9013R airfoil lattice at $\pi = 0.3$ $\delta = 0.3$ was carried out using the Reynolds Stress turbulence model. A numerical study of the spatial flow in the interscapular channel has been carried out. As a result of the calculations performed, the flow patterns in the interscapular channel and behind it were obtained. The distribution of the kinetic energy loss coefficients along the grating front at various degrees of opening of the diaphragm at the inlet to the nozzle apparatus. The results obtained in this work will develop a method for multi-parameter optimization of cogeneration steam turbines with controlled steam extraction.

Keywords: Supersonic flow · Rotary diaphragm · Blade channel · Energy efficiency

1 Introduction

Continuous development and improvement of the design and operating modes of cogeneration turbines have led to the use of steam with supercritical parameters. At this point in time, one of the promising trends in developing thermal power turbines is their operation at supercritical pressure drops [1]. An increase in the steam parameters entails an increase in the flow rates in the inter-blade channels of the nozzle and working channels. In this case, it is necessary to reprofile the flow path to obtain the optimal geometry with the lowest kinetic energy loss coefficients. The development of optimization methods for the flow path of heating turbines is an urgent task.

V. Ivanov et al. (Eds.): DSMIE 2022, LNME, pp. 66–78, 2022.
https://doi.org/10.1007/978-3-031-06044-1_7

2 Literature Review

A large number of works are devoted to investigations of transonic and supersonic flows in channels (reflux channels [2, 3] and other channels [4–7]). But a feature of cogeneration turbines with adjustable steam extraction is the use of nozzle grids with rotary diaphragms [4]. The change in the steam flow rate through the turbine under variable modes is achieved by overlapping, at the inlet, the nozzle apparatus channels (Fig. 1). The part of the nozzle that blocks the inlet channel is called the rotary diaphragm.

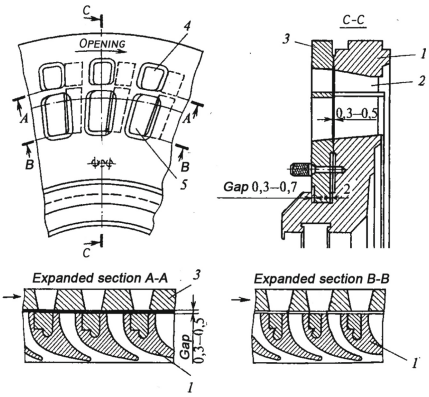

Fig. 1. Regulating turbine diaphragm: 1 - diaphragm; 2 - nozzles; 3 - rotary ring; 4 and 5 – windows.

The flow structure in the nozzle array channel is greatly influenced by the degree of opening of the diaphragm δ [8]. Here $\delta = \frac{a}{a_0}$ – the degree of opening of the rotary diaphragm is the ratio of the area of the closed rotary diaphragm to the area of the fully open diaphragm (Fig. 2).

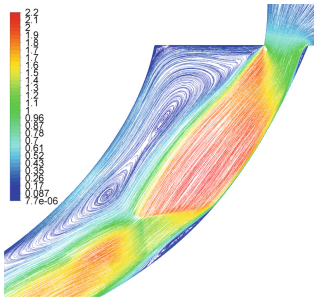

Fig. 2. Flow in the computational domain. Isolines of Mach numbers at $= \pi = 0{,}3\ \delta = 0{,}3$.

In the process of developing a method for the numerical study of a plane flow around a nozzle array with a rotary diaphragm, calculations were performed at various degrees of opening of the rotary diaphragm δ and pressure drops π across the array. As a result of calculations, for small degrees of opening of the rotary diaphragm, complex flow patterns were obtained in the blade channel of the nozzle, with the division of the flow core into supersonic regions, shown in Fig. 2. An additional numerical analysis was carried out for a more detailed study of these phenomena. The paper presents some results of a numerical study of supersonic flow in the channel of the nozzle apparatus at the degree of opening of the rotary diaphragm $\delta = (0{,}15 \div 0{,}3)$.

Numerical studies were carried out using the ANSYS Fluent software package.

3 Research Methodology

The computational area is one blade channel formed by the back and the trough of the C-9013R profile developed by MEI (Fig. 3). The main requirement for the computational grid is a high-quality resolution of physical phenomena occurring in the computational domain [9, 10]. On the one hand, the grid must ensure the resolution of phenomena in the boundary layer of the near-wall region and phenomena in the flowing part of the lattice, and beyond it, arising at transonic and supersonic flow rates (shock waves, flow separations, wakes), which requires densification of the mesh in the indicated areas. On the other hand, the size of the grid cells should be limited in terms of the time spent on performing the calculations.

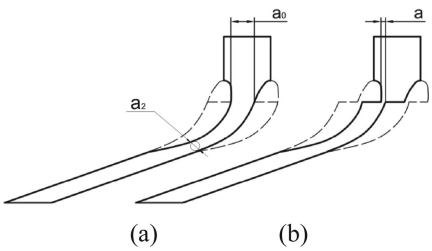

Fig. 3. Computational area for the S-9013R profile at $\delta = 1$ (a) and $\delta = 0{,}15$ (b).

The computational domain can be divided into two parts: movable, limited by the rotary diaphragm, and fixed, limited by the interscapular channel behind the rotary diaphragm. In this connection, it is possible to construct separate meshes for these areas once and then, using a non-conformal interface, move them relative to each other, simulating different degrees of diaphragm opening δ. In practice, due to the need to compact the mesh at the walls to meet the requirements for the value of $y^+ \approx 1$, a poorly matching and curved interface is obtained. Test calculations showed the presence of “discontinuities” and “jumps” on the isolines of the parameters, which forced to abandon the use of the non-conformal interface.

Further, its own grid was built for the computational domain for each of the selected degrees of opening of the rotary diaphragm. Considering all of the above, the following approach was applied when constructing the mesh in the computational domain. Since the position of the shock waves and flow separations in and behind the channel is unknown, the grid was built to ensure the condition $y^+ \approx 1$ in the near-wall region.

The thickness of the boundary layer was divided into 25 sublayers, with an element magnification factor of 1.2. The rest of the mesh was set equal to the cell size in the last sublayer. As a result, the number of mesh elements ranged from $1,8 \cdot 10^5$to $2,4 \cdot 10^5$, depending on the degree of opening δ.

The preliminary results obtained (Fig. 4) required more detailed studies of the flow in the channels of the gratings with rotary diaphragms:

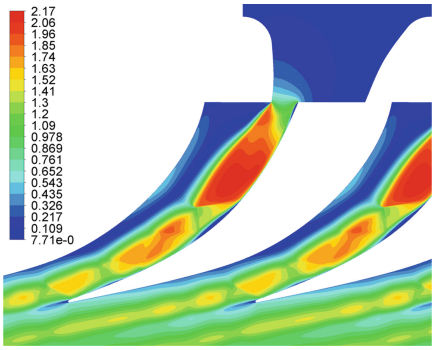

Fig. 4. Flow in the computational domain. Isolines of Mach numbers at $\pi = 0.3$, $\delta = 0.3$, k-ω SST turbulence model.

1. A numerical study of the flow in the blade channel of the C-9013R profile lattice at $\pi = 0.3$ $\delta = 0.3$ was carried out using the Reynolds Stress turbulence model. The model is used to simulate turbulence and makes it possible to obtain a good agreement between the results of the calculation of supersonic jet flows with the experiment's results [11]. Since the model uses near-wall functions to resolve the phenomena in the boundary layer, a separate computational domain was built with a mesh satisfying the condition $y^+ \leq 30$ with the number of elements ≈63000 pcs.

   In Fig. 5 shows the flow pattern obtained in the calculation using the Reynolds Stress turbulence model. As can be seen from the figure, the flow pattern in the blade channel obtained by analysis using the Reynolds Stress turbulence model is similar to the previously obtained flow pattern calculated using the k-ω SST turbulence model (Fig. 4).
2. Additionally, to assess the possible influence of the profile shape on the flow pattern in the interscapular channel formed from profiles No. 99 developed by TsAGI. The profile was chosen because of the similarity to the C-9013R profile in terms of geometric characteristics. $t/b = 2$. For profile No. 99, a computational domain was constructed, corresponding to the degree of opening of the rotary diaphragm $\delta = 0.3$. The calculation was performed using the k-ω SST turbulence model with the same

settings of the Fluent CFD solver as for the C-9013P profile. The flow pattern in the blade channel of the lattice of profiles No. 99 is shown in Fig. 6. As can be seen, in the blade channel, there are regions similar to the regions obtained when calculating the flow for the C-9013R profile lattice.

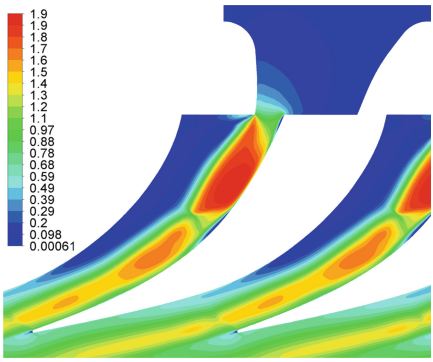

Fig. 5. Flow in the computational domain. Isolines of Mach numbers at $\pi = 0.3$, $\delta = 0.3$, Reynolds Stress turbulence model.

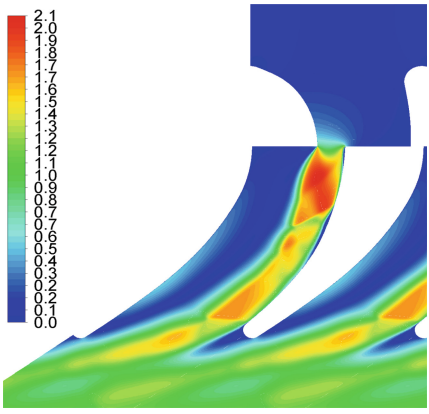

Fig. 6. The flow in the computational region of the blade channel of the lattice of profiles No. 99. Isolines of Mach numbers at $\pi = 0.3$, $\delta = 0.3$, turbulence model k-ω SST.

3. A numerical study of the spatial flow in the blade channel has been carried out. For this, the blade channel of the nozzles was simulated with a diaphragm opening of $\delta = 0.3$ to calculate the spatial flow. The channel height was 80 mm (l/b = 1.3). In the computational domain, a mesh of Poly-Hexcore elements was built (MosaicTM technology, which allows you to construct a mesh consisting of hexagonal prisms in the wall area and to carry out a direct transition from a polyhedral mesh to a hexahedral mesh bypassing tetra-cells) (Fig. 7).

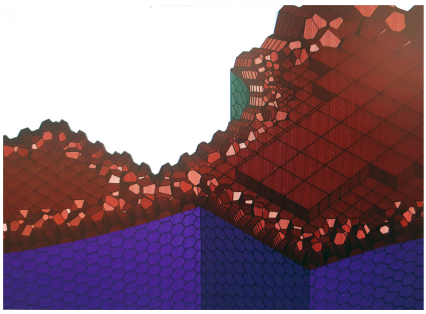

Fig. 7. *Poly-Hexcore* mesh in the computational domain for the C-9013P profile at $\delta = 0{,}3$.

Since the main task was to confirm the previously obtained flow pattern in the blade channel, without calculating the kinetic energy loss coefficients, the computational domain was divided into a relatively small number of elements - a little more than 8 million. All solver settings are the same as for plane flow simulations, using the k-ω SST turbulence model. The flow pattern in the plane at the height of 40 mm is shown in Fig. 8.

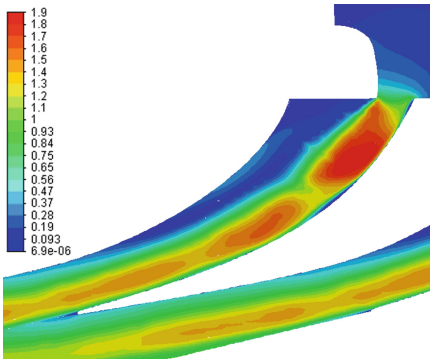

Fig. 8. Flow in the computational domain. Isolines of Mach numbers at $\pi = 0{,}3$, $\delta = 0{,}3$.

In all three cases of the verification calculation, a flow pattern was obtained in the blade channel with the division of the flow core into supersonic regions. Based on this, a conclusion was made about the presence of similar phenomena in a real nozzles, and a decision was made to conduct an additional study of the flow in the blade channel of a nozzles with a rotary diaphragm at low degrees of opening.

For the numerical study of the plane flow, we used the model of a two-dimensional viscous gas flow of the CFD solver Fluent using a second-order difference method. The working fluid is a viscous compressible gas - air. To calculate the turbulence phenomena, the k-ω SST turbulence model (Menter's model) [12] was used. The following were used as boundary conditions at the entrance to the computational domain: air pressure and temperature, for some part of calculations, airflow and temperature; airflow direction; the intensity of turbulence; hydraulic diameter.

Air pressure was set as the boundary condition at the exit from the computational domain. All calculations were performed in two stages. A "rough" flow calculation was performed using the FMG utility. The FMG utility uses the ANSYS FLUENT FAS Multigrid technology to perform calculations on a set of sequentially nested grids. The calculation starts on the coarsest grid, and the results are interpolated to the next finer grid as it settles. As a rule, all "rough" calculations, to achieve residual values 10^{-6}, required no more than 1000 ÷ 2000 iterations. According to the "rough" calculation results, the mesh was adapted in places of large gradients of the calculated parameters and to ensure the condition $y^+ \leq 1$. The adaptation resulted in a mesh with suspended nodes. For "finishing" calculations, depending on the values of M and δ, the amount of iterations was 20,000 ÷ 33,000 pieces. The convergence of the calculation was assessed by establishing the equality of the flow rates at the inlet and outlet from the computational domain and by establishing the residuals of the kinetic energy loss coefficient.

4 Results

To apply one of the theories describing the phenomena in supersonic flow, it is necessary to solve the problem of the type of flow in the blade channel. On the one hand, this is undoubtedly a supersonic flow in the turning channel; on the other hand, due to the sudden expansion after the turning diaphragm, part of the flow can be considered as the outflow of a supersonic jet into a cavity with pressure almost equal to the pressure in the jet.

It is also possible to distinguish two flow regimes in the computational domain. In the first case, the minimum area is in the throat a_2 of the blade channel (Fig. 2) - confusor flow in the channel. In the second case, at low degrees of opening δ, when the ratio τ of the channel width at the inlet a to the throat of the grating a_2 becomes less than unity - the diffuser flow in the channel. In Fig. 10 shows the dependence of the flow rate ratio on the ratio τ of the channel width at the inlet a to the throat of the grating a_2. As can be seen from the graph (Fig. 9), throttling of the flow begins to occur at values of $\tau > 1$.

Thus, at $\tau = 1.7$, the ratio of the flow rates through the nozzle apparatus is G/G0 $= 0.99$; at $\tau = 1.4$, the ratio G/G0 $= 0.97$, etc. In this case, the ratio of the flow rates through the nozzle G/G0 does not depend on the pressure difference π on the cascade for the same values of τ (δ).

In Fig. 10 shows the calculated area for the degree of opening $\delta = 0.3$ with the indication of the dashed line, which is the equidistant profile of the trough of the blade with straight sections at the inlet and outlet, along which π is measured as the ratio of the static pressure to the total pressure. Since the condition of equality of the flow rates at the inlet and outlet from the grating must be observed, in the case of a diffuser flow, a local increase in the velocity in the flow core occurs in the channel to compensate for the decrease in the flow area due to the overlap of the rotary diaphragm. As can be seen from the graph in Fig. 10, the pressure ratio immediately after the rotary diaphragm is significantly less than the critical value (0.525).

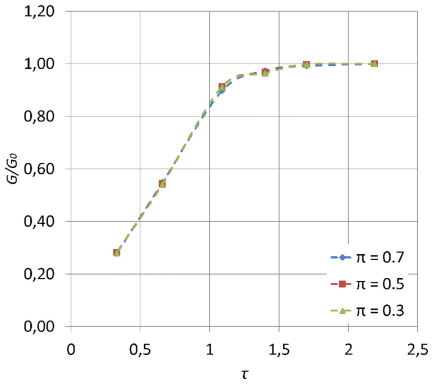

Fig. 9. Dependence of the ratio of airflow rates through the nozzle device G/G0 on τ.

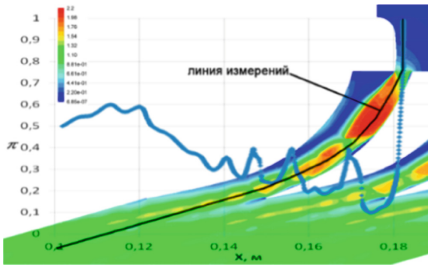

Fig. 10. Distribution of the static pressure ratio to total pressure along the channel at $\pi = 0{,}3$ and $\delta = 0{,}3$.

Further, the pressure ratio gradually increases as the flow moves towards the outlet from the grid. In this case, the flow rate decreases. That is, the flow moves against a positive pressure gradient. In this case, the interscapular channel is divided into two regions: at the trough of the blade, there is a region of supersonic flow. There is a region of the vortex at the back of the blade, subsonic flow. This is confirmed by the distribution of Mach numbers (Fig. 4) and the position of the regions with a critical drop along the interscapular channel (Fig. 11).

To simplify the description of the phenomena in the channel, we denote the flow regions (Fig. 11). After the flow passes through the rotary diaphragm, the flow in the ABC triangle occurs similarly to the flow in the oblique cut of the nozzle apparatus. Since the pressure in front of the rotary diaphragm is greater than behind it (Fig. 11), the expansion of the gas occurs in the oblique cut ABC, which thus plays the role of the expanding part of the nozzle.

Since the pressure in front of the rotary diaphragm is greater than behind it (Fig. 11), the expansion of the gas occurs in the oblique cut ABC, which thus plays the role of the expanding part of the nozzle. The process of gas expansion in a diagonal cut is as follows. Since the pressure gradually drops from P_{cr} in section AB to P_{in} section AC, the isobars corresponding to intermediate pressures are located approximately in the form of rays emanating from point A. Thus, in section BC, the pressure decreases gradually,

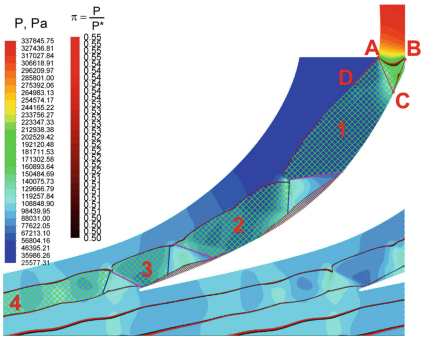

Fig. 11. Distribution of static pressure and critical pressure ratio in the interscapular channel at $\pi = 0{,}3$ and $\delta = 0{,}3$.

while at point A the pressure drops instantly from P_{cr} to P, and, consequently, along with the line AD, which is the boundary of the jet, the pressure will be equal to P. Under the influence of this pressure difference, a resulting force appears at the boundary of the jet, directed perpendicular to the axis of the channel, which turns the flow by a certain angle. As a result of this rotation, the width of the jet increases, and an expanding nozzle is obtained, which can trigger a supercritical pressure drop [13]. This is what happens in region 1.

Further, since the flow moves against a positive pressure gradient, that is, the pressure in the flow should gradually become equal to the pressure behind the nozzle apparatus, a shock front appears (shown by a pink line) representing a compression wave, pressure, and the gas density in it increases. The shock front begins on the wall, obliquely to it, and is accompanied by the jet's separation from the blade's trough (the red shading shows the separations). Having reached the jet boundary, the shock front is reflected from it, and a reflected front appears (shown by the blue line). In this case, the reflected shock front is a rarefaction wave, and the jet boundary diverges again. Then the whole process is repeated - regions 2 and 3. By the action of viscosity at the boundary of the jet, this periodic pattern is finally erased - region 4 [14, 15].

To determine the value of the relative pressure drop across the nozzle apparatus, at which the flow core is divided by shock fronts into separate regions, shown in Fig. 11, additional calculations were performed at relative pressure drops across the nozzle array $\pi = 0.5; 0.45; 0.4; 0.35; 0.3$ (Fig. 12).

As a result of the performed calculations, it was found that for the degree of opening $\delta = 0.3$ ($\tau = 0.66$), the division of the flow core of the region by shock fronts into regions begins at a relative difference of $\pi = 0.4$. Real nozzle devices with rotary diaphragms operate with steam extraction in the cavity in front of the nozzle device. A significant influence on the nature of the processes in the flow path of the turbine, the efficiency of the nozzle grids of adjustable rotary diaphragms and their stages, as well as on the integral quality indicators of the entire turbine, the pressure levels in the chambers of controlled extraction and the values of the mass flow rates of the extracted steam was confirmed [16]. In this connection, a numerical study of the influence of the amount of air intake on the nature of the flow and the loss of kinetic energy in the lattice was

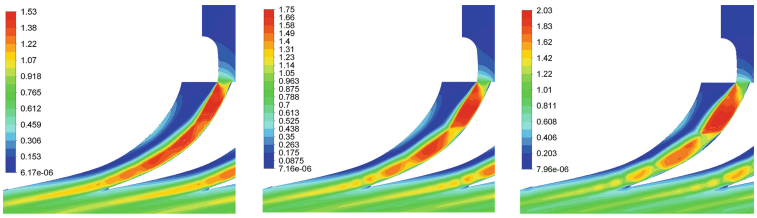

Fig. 12. Flow in the computational domain. Isolines of Mach numbers at a) $\pi = 0{,}45$ and $\delta = 0{,}3$; b) $\pi = 0{,}4$ and $\delta = 0{,}3$; c) $\pi = 0{,}35$ and $\delta = 0{,}3$.

carried out. Calculations were carried out for the values of withdrawals G/G0 = 1; 0.75; 0.6875; 0.625; 0.5 at degrees of opening of the rotary diaphragm $\delta = 0.3$; at $\pi = 0.3$. In Fig. 10 shows the dependence of the coefficient of kinetic energy losses in the nozzle array on the amount of air intake. As shown from Fig. 13, losses increase with increasing air intake in front of the nozzle apparatus.

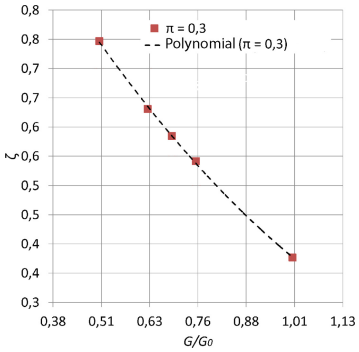

Fig. 13. Dependence of the coefficient of kinetic energy losses on the amount of withdrawals G/G_0.

With a decrease in the airflow value ahead of the nozzle apparatus, the flow pattern changes in the same way as with a decrease in the relative pressure difference π. The division of the flow core by shock fronts into separate regions begins at the ratio G/G0 = 0.6875. In Fig. 14 shows the distribution of the kinetic energy loss coefficients along the front of the grating at the degree of opening of the rotary diaphragm $\delta = 0.3$ at different relative pressure drops across the grating.

Analysis of the graph indicates that the loss of kinetic energy decreases with increasing flow rate, with smaller relative differences in π. In relative terms, the lattice's kinetic energy loss coefficient is 22.5% higher at $\pi = 0.7$ than at $\pi = 0.3$. In Fig. 15 shows the isolines of the Mach numbers in the interscapular channel at $\pi = 0.7$; 0.3 and $\delta = 0.3$.

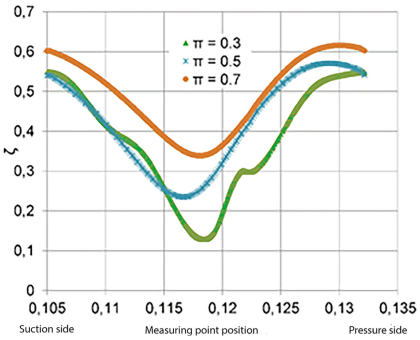

Fig. 14. Distribution of kinetic energy loss coefficients along the lattice front at $\pi = 0{,}3$; 0,5; 0,7 and $\delta = 0{,}3$.

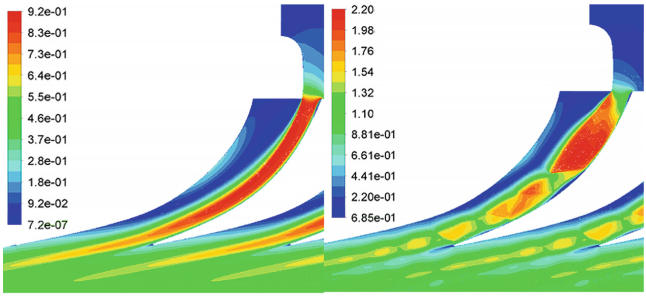

a) b)

Fig. 15. Isolines of Mach numbers in the interscapular channel at $\pi = 0{,}7$ (a) and $\pi = 0{,}3$ (b).

The figures show that with a decrease in the relative pressure drop across the lattice, the vortex flow region decreases, and, accordingly, the flow core increases. Considering the above, to Fig. 14 it can be concluded that a decrease in the vortex zone and an increase in the flow core lead to a decrease in the kinetic energy losses in the lattice. In [17], it is indicated that to reduce the length of the zone of separated flows with partial openings of the diaphragms, the rotary ring should be moved to the closing position (in contrast to the method traditionally used in turbines) in the direction from the concave (trough) to the convex surface (back) of the nozzle channel, and in the open position - in the opposite direction. A numerical study was carried out to determine the coefficient of kinetic energy losses, with the opening degree $\delta = 0.3$ and the position of the movable part of the rotary diaphragms, as indicated above. The flow pattern in the interscapular channel of the nozzle apparatus at $\pi = 0.3$ in Fig. 16.

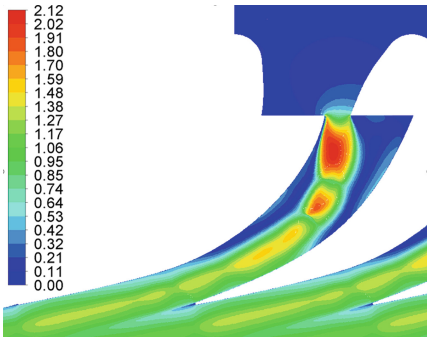

Fig. 16. Isolines of Mach numbers in the interscapular channel at $\pi = 0{,}7$ (a) and $\pi = 0{,}3$ (b).

5 Conclusions

Based on the results of the work carried out, the following conclusions can be drawn: throttling of the flow passing through the rotary diaphragm of the nozzle apparatus begins to occur when the values of the ratio of the channel width at the entrance to the throat of the grating are greater than unity; the structure of the flow in the interscapular channel of the nozzle apparatus at low degrees of opening is divided into two parts: the supersonic core at the blade trough and the subsonic vortex zone at the blade back; the supersonic core of the flow at specific values of the relative pressure difference across the cascade (or the value of the air flow through the cascade) is divided by shock fronts into several regions; the coefficients of energy losses, for small degrees of opening, decrease with a decrease in the relative pressure drops (with an increase in the flow rate of the flow from the nozzle array); the greatest contribution to the amount of kinetic energy losses is made by the vortex zone in the interscapular channel, and not by wave phenomena in the flow core. Optimization of the flow path of the nozzle apparatus must be carried out to reduce the areas with vortex flow. The results obtained in this work will be used to develop a method for multi-parameter optimization of cogeneration steam turbines with controlled steam extraction.

References

1. Kondrat'ev, A., et al.: Development of steam turbines for supercritical and supersupercritical gas parameters. Bull. Bryansk State Tech. Univ. **1**(54) (2017)
2. Wang, Y., Yu, Y., Hu, D.: Experimental investigation and numerical analysis of separation performance for supersonic separator with novel drainage structure and reflux channel. Appl. Therm. Eng. **176**, 115111 (2020). https://doi.org/10.1016/j.applthermaleng.2020.115111
3. Ma, C., Wang, Y., Yu, Y., Ren, W., Hu, D.: Structure improvements and performance study of Supersonic Separation device with reflux channel. Chem. Eng. Process. Process Intensif. **138**, 73–85 (2019). https://doi.org/10.1016/J.CEP.2019.03.009
4. Yang, X., Fu, P., Chen, N., Liu, J., Wei, J.: Mechanisms of pressure pulse for condensing supersonic steam jet in a rectangular channel. Exp. Therm. Fluid Sci. **105**, 223–233 (2019). https://doi.org/10.1016/J.EXPTHERMFLUSCI.2019.04.003

5. Li, Q., Lyu, Y., Pan, T., Li, D., Lu, H., Gong, Y.: Development of a coupled supersonic inlet-fan Navier-stokes simulation method. Chinese J. Aeronaut. **31**, 237–246 (2018). https://doi.org/10.1016/J.CJA.2017.11.011
6. Penzin, V.: Deceleration of the Supersonic Flow in the Channels. Centeral Aero-Hydrodynamic Institute, Moscow (2012)
7. Merzliakov, I., Pavlenko, I., Chekh, O., Sharapov, S., Ivanov, V.: Mathematical modeling of operating process and technological features for designing the vortex type liquid-vapor jet apparatus. In: Ivanov, V., et al. (eds.) DSMIE 2019. LNME, pp. 613–622. Springer, Cham (2020). https://doi.org/10.1007/978-3-030-22365-6_61
8. Slabchenko, O., Kirsanov, D.: Results of calculating the flow in the channels of the regulating rotary diaphragm of the heating turbine NTU "KhPI". Bull. Ser. Power Heat Eng. Process. Equip. **6**, 73–75 (2008)
9. Ershov, S., Yakovlev, V.: Influence of the grid resolution on the results of calculating three-dimensional flows in the flow paths of turbomachines using RANS models. Probl. Mech. Eng. **18**(4/1), 18–24 (2015)
10. Hu, W.J., Tan, K., Markovych, S., Liu, X.L.: Study of a cold spray nozzle throat on acceleration characteristics via CFD. J. Eng. Sci. **8**(1), F19–F24 (2021). https://doi.org/10.21272/jes.2021.8(1).f3
11. Glushko, G., Ivanov, I., Kryukov, I.: Simulation of turbulence in supersonic jet streams. Physicochem. Kinet. Gas Dyn. **9**, 1–8 (2010)
12. Avdieieva, O., Usatyi, O., Mykhailova, I.: Optimization of the flowing part of the turbine K-310-240 based on the object-oriented approach. In: Machado, J., Soares, F., Trojanowska, J., Ottaviano, E. (eds.) icieng 2021. LNME, pp. 201–213. Springer, Cham (2022). https://doi.org/10.1007/978-3-030-79165-0_20
13. Boiko, A., Govorushchenko, Y.: Optimization of the Axial Turbines Flow Paths. Science Publishing Group, New York (2016)
14. Razaaly, N., Persico, G., Congedo, P.M.: Impact of geometric, operational, and model uncertainties on the non-ideal flow through a supersonic ORC turbine cascade. Energy **169**, 213–227 (2019). https://doi.org/10.1016/J.ENERGY.2018.11.100
15. Kelin, A., Larin, O., Naryzhna, R., Trubayev, O., Vodka, O., Shapovalova, M.: Estimation of residual life-time of pumping units of electric power stations. In: 2019 IEEE 14th International Conference on Computer Sciences and Information Technologies (CSIT), pp. 153–159. Lviv, Ukraine (2019). DOI: https://doi.org/10.1109/STC-CSIT.2019.8929748
16. Boyko, A.V.: Complex mathematical model of processes in a turbine with controlled steam extraction Bulletin of NTU "KhPI". Ser. Energy Heat Eng. Process. Install. **8**(1180), 28–36 (2016)
17. Drokonov, A., Drokonov, A.: Improvement of regulating diaphragms of steam turbines. Bull. Bryansk State Techn. Univ. **2**(46), 26–31 (2015)